ARMA 16-413

Effect of Confining Stress on Sand-Fiber Proppant Placement in a Deformable Fracture

Medina, R. and Detwiler, R.L.
University of California Irvine, Irvine, CA, USA
Prioul, R. and Xu, W.
Schlumberger-Doll Research Center, Cambridge, MA, USA
Ortega, J. A.
Schlumberger, Houston, TX, USA

ABSTRACT: We applied a normal stress ($\sigma_n = 0 - 12.8$ psi) to a transparent deformable fracture to investigate the behavior of sand-fiber mixtures. Using light transmission techniques, we quantified the sand volume fraction ϕ_s throughout the experiment. In the absence of an applied normal stress, $\sigma_n = 0$, the sand and fibers settled into randomly distributed sand-fiber islands. Injecting solids-free carrier fluid displaces the settled solids washing them out of the fracture. Results for applied-normal stress experiments ($\sigma_n = 0 - 12.8$ psi) demonstrate the sand-fiber islands compacted and the solid volume within them increased as σ_n increased. We observed that these sand-fiber islands supported the applied normal stress and prevented fracture closure, acting as pillars between the fracture surfaces. After injecting solids-free carrier fluid, while keeping σ_n =12.8 psi, we observed most sand-fiber pillars remained in place and some solids-free pathways were created. The formation of such pathways shows that the addition of fibers to hydraulic fracturing fluids, even at small concentrations, may increase fracture permeability through the formation of sand-fiber pillars capable of supporting a normal stress, preventing fracture closure.

1. INTRODUCTION

Settling of non-Brownian particles in polymeric fluids (e.g., xanthan or guar gels) is of great importance for many different industrial applications, especially in industries where the aim is to prevent particles from settling or at least decrease the settling rate of the particles, e.g., oil and gas production and well drilling operations. Recently, it has been proposed that the addition of rod-like solids (e.g., fibers) to polymeric fluids may reduce particle settling rates. Elgaddafi et al. (2012) have previously demonstrated a settling rate reduction of a single particle falling through a suspension of dispersed fibers. Much of the recent work has focused on the influence of fibers on the rheological properties of the suspension (George et al., 2011; George et al., 2012; Guo et al., 2005; Rajabian et al., 2008). These studies have shown that adding fibers to a polymeric fluid will increase the apparent viscosity of the fluid and reduce settling rate. The reduced settling rate was attributed to the formation of intertwined networks of fibers and polymeric glucose-chains (Guo et al., 2005; Rajabian et al., 2008). Previous research characterized the settling of dispersed sand (Chhabra and Peri, 1991; Guazzelli and Hinch, 2011; Happel and Bart, 1974) and dispersed fibers (Baldock et al., 2004; Herzhaft and Guazzelli, 1999; Herzhaft et al., 1996) suspensions. However, there is limited literature for the suspension and settling of sand-fiber mixtures.

The focus of the work presented here is to investigate the behavior of semi-dilute suspensions of sand and fibers settling inside a parallel-wall fracture subjected to a normal stress, σ_n. We are interested in the regime where the fracture aperture is on the same order of magnitude as the fiber length; these dimensions are within the range of dimensions encountered in hydraulic fracturing operations. Whereas hydrodynamic interactions typically dominate the behavior in a system of dispersed particles, it is expected that fiber-fiber, sand-fiber, and sand-sand contacts will dominate over hydrodynamic interactions and control the settling behavior. We expect that the formation of intertwined fiber-polymer networks will lead to the

entrapment of sand particles, forming sand-fiber-polymer islands. Upon loading, these islands compact and form pillars that can now support the applied normal stress. Because these pillars are separated by areas of open fracture, use of sand-fiber proppant mixtures has the potential to yield higher fracture permeability than sand-only proppant while requiring less solid material.

2. EXPERIMENTAL SETUP

The experiments were carried out in a vertically oriented transparent fracture. The experimental setup (see Fig. 1) includes a rotating stand housing a high-resolution CCD camera (Quantix KAF-6303e), red LED backlight, electronic controllers, and the fracture cell; additionally, we use a pneumatic tank to inject the slurry into the fracture and a laboratory scale to measure effluent mass flow rate. A detailed schematic and a photograph of the fracture cell are shown in Fig. 2. The transparent fracture was composed of two 15.2 $\times$ 15.2 $\times$ 1.2 cm flat pieces of glass sealed by four manifolds: two no-flow manifolds (top and bottom, in red), inlet (left, in blue), and outlet (right, in blue) manifolds. The fracture is secured between two aluminum frames with fused-quartz windows by placing one clear PVC-gasket on the top and bottom of the fracture. Eight reverse-action pneumatic-actuators (Bimba SR-092-R) were rigidly mounted on the top aluminum frame with their steel rods securely screwed to the bottom frame. Supplying air pressure to the actuators forced the rods to retrieve into the cylinder, pulling the two aluminum frames towards each other, forcing fracture closure. Four linear variable displacement transducers (LVDT, Schaevitz HCD 250) rigidly mounted on opposite sides (two on each side) of the fracture cell accurately ($\pm 1 \mu m$) measured fracture aperture changes throughout the experiment.

2.1. *Experimental Procedure*

The carrier fluid was prepared by mixing deionized de-aired water, guar-gum (0.48% W/W), and glutaraldehyde (0.01% V/V) in a laboratory-grade blender operating at 6,800 rpm. The solution was mixed for several minutes before increasing the blender speed to 16,900 rpm; mixing continued for $\sim$10 minutes. The carrier fluid was then placed under vacuum for approximately 12 hours to remove air bubbles and ensure complete hydration of guar. This guar-water mixture yields a shear thinning fluid with an apparent viscosity of μ=1.2 Pa·s at a shear rate of $\dot{\gamma}$=0.1 s^{-1}. A detailed description of the preparation of the carrier fluid was provided by Medina et al. (2015).

The suspension was prepared by slowly adding 40/70-mesh silica sand (particle radius ranging from $a = 0.13 - 0.24$ mm) and polymeric fibers (fiber length $l \approx 10 \pm 2$ mm

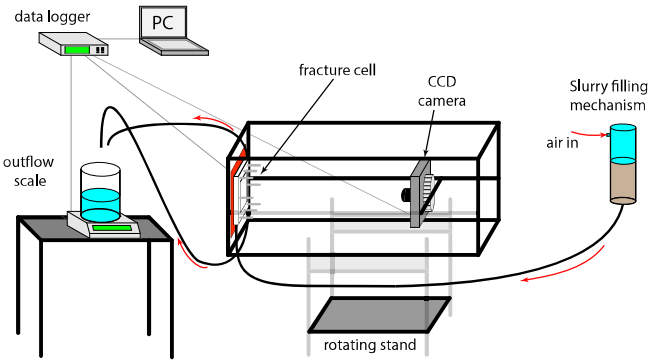

Fig. 1: Schematic of experimental system. The slurry-filling mechanism consisted of a pneumatic tank, PVC pipe with a fitted funneled end-cap. After the slurry is poured into the pneumatic tank, air is supplied at a given pressure and the slurry is then displaced and injected into the fracture. Once a steady-state flow rate was achieved, the flow was stopped and slurry allowed to settle inside the fracture cell (See Fig. 2 for details). After the slurry settled for some predetermined time, a normal stress was applied to the fracture-cell by activating the pneumatic actuators.

and diameter $d \approx 12 \pm 2 \mu$m) into the carrier fluid using a rotary mixing paddle. The suspension was prepared by initially adding $\sim 30\%$ of the total sand and slowly adding fibers while the rotary paddle mixed the suspension. Once $\sim 60 - 80\%$ of the fibers were in solution, we added additional $\sim 30\%$ of sand, mixed for several minutes, and finally added the remaining fibers and sand. Adding solids in small amounts before and during the fiber mixing helps disperse the fibers in solution. The final suspension had a total solid volume fraction of $\phi_{\text{total}} = \phi_s + \phi_f = 0.1808$, with most of the solid volume fraction made up of sand particles ($\phi_s = 0.177$) and fibers making up the remainder of the solid volume fraction ($\phi_f = 0.0038$).

We carried out four different experiments (Tests A-D) to investigate the settling behavior of sand-fiber mixtures. All experiments were initialized using the same procedure. Initially, the fracture and all associated tubing (from the pneumatic tank to the outlet) were filled with carrier fluid; a set of reference images were acquired with the cell completely filled with carrier fluid. Image acquisition began before injecting the suspension to capture the entire process, i.e., initial filling and settling. Immediately after mixing, the suspension was transferred to a pneumatic tank and injected into the fracture until $\sim$10 fracture volumes had passed through the system. In test A (no applied normal stress, $\sigma_n = 0$), we allowed solids to settle for approximately 2 hours (previously conducted experiments in a constant-aperture fracture demonstrated negligible settling or solid distribution changes after $\sim$1.5 hours). After 2 hours, we injected solids-free carrier fluid at a flow rate of $100 - 300$ ml min^{-1} for up to 25 fracture volumes. For Tests B-D (applied normal stress $\sigma_n = 0 - 12.8$ psi),

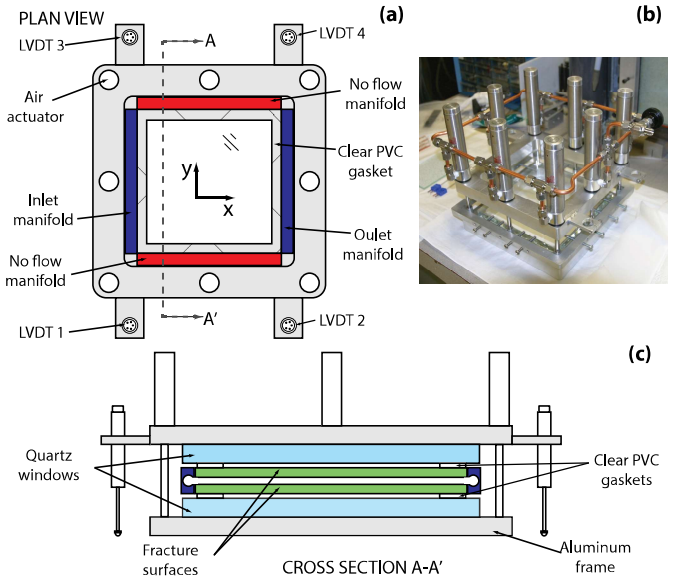

Fig. 2: Schematic and photograph of the fracture cell used in our experimental system. (a) Plan view of the fracture cell showing the location of all eight pneumatic-actuators, linear variable differential transducers (LVDT) and inlet and outlet manifolds; (b) photograph of the fracture cell; and (c) cross-section view (A-A') of the fracture cell showing the fracture walls and inlet/outlet manifold configuration. For all experiments, flow was along the x-axis and gravity points in the negative y-direction.

we allowed the suspension to settle for ∼25 minutes before applying the first normal stress; we incrementally increased normal stress, σ_n, at regular time intervals of ∼50 minutes, from 1.8 psi (12.4 kPa) to a maximum of 12.8 psi (88.3 kPa). We maintained $\sigma_n = 12.8$ psi and proceeded to inject solids-free carrier fluid at flowrates ranging from 100-300 ml min^{-1}.

3. IMAGE ANALYSIS

Light transmission techniques allowed us to accurately measure the fracture aperture field, b_{ij}. We take two reference images, one with the fracture filled with deionized water and one with the fracture filled with dyed water at a known concentration. The raw intensities are then used to calculate the absorbance field using Beer-Lambert law ($A_{\text{dye}} = \ln(I_c/I_d) = \xi(C_c - C_d)b$), where I is the light intensity, ξ is the absorptivity coefficient, C is the solute concentration, b is the aperture, and subscripts c and d denote the clear and dyed solution, respectively. The aperture field is then calculated using an independently measured mean aperture by (for more details see Detwiler et al. (1999)):

$$b_{ij} = \frac{A_{\text{dye}_{ij}}}{\langle A_{\text{dye}} \rangle} \langle b \rangle \tag{1}$$

where b_{ij} is the aperture at fracture location (i, j), A is the absorbance, and $\langle \cdot \rangle$ is a spatial average. The mean and standard deviation of the initial aperture field for all experiments are given in Table 1.

Table 1: Mean ($\langle b \rangle$) and standard deviation σ_b of the initial aperture field for all four experiments.

	$\langle b \rangle [\mu m]$	$\sigma_b [\mu m]$
Test A	2895.4	130.0
Test B	3114.7	161.2
Test C	2865.4	174.0
Test D	2692.5	110.7

3.1. *Solid Volume Fraction Estimation*

We carried out an independent test inside a constant-aperture fracture to measure light absorbance by a sand-filled fracture at a known solid volume fraction. A concentrated suspension was prepared using a procedure similar to that described in Section 2.1. The suspension was prepared with silica sand (40/70-mesh) at a solid volume fraction of $\phi_s = 0.5$. The suspension was injected into the constant-aperture fracture and allowed to settle, undisturbed, for 6 days. Settling for an extended period of time ensures that the settling solids reach a steady-state configuration. Settling was undisturbed, i.e., no shaking; therefore, we expect that at the end of the settling experiment, the solid concentration inside the fracture had reached a value close to the random loose packing limit, $\phi_s \to \phi_{\text{rlp}} \approx 0.55$ (Shapiro and Probstein, 1992).

Following light absorption and scattering theory for a "slab" of particles (Bohren and Huffman, 2008) a relationship between the light absorbance and particle concentration in the fracture can be written as:

$$A = n_s C_{\text{ext}_s} b \tag{2}$$

where b was previously defined and the absorbance is now defined as $A = \ln(I_{cf}/I_s)$, where I_{cf} and I_s are the light intensity through the carrier fluid and sand, respectively. n_s is the particle density of the sand (i.e., number of sand particles per unit volume), and C_{ext_s} is the extinction cross section of the sand particles. The extinction cross section is a measure of total light attenuated by the particle which includes attenuation due to light scattering and absorption. For spherical particles, the particle density is defined as $n_s = \phi_s \frac{3}{4\pi a^3}$, and Eq. 2 can be rewritten as

$$A = \phi_s \left(\frac{3 C_{\text{ext}_s}}{4\pi a^3} \right) b \tag{3}$$

Eq. 3 is further simplified to $A = \phi_s \alpha_s b$, by defining α_s as the absorbance coefficient, i.e., absorbance attenuation per unit length. From the experiment described above, we can estimate the absorbance coefficient; this is because the particles settled uniformly inside the constant-aperture

fracture (without fibers) and $\phi_s \approx \phi_{rlp}$:

$$\alpha_s = \frac{A_{ij}}{\phi_s b_{ij}} \approx \frac{A_{ij}}{\phi_{\text{rlp}} b_{ij}} \tag{4}$$

Using the measured absorbance of the settled sand and the aperture, we calculated the mean value of the absorbance coefficient of 40/70-mesh silica sand to be $\langle \alpha_s \rangle = 1.3 \times 10^{-3}/\mu$m with a standard deviation of $\sigma_{\alpha_s} = 6.9 \times 10^{-5}$. Because light absorption is linearly dependent on all components attenuating light through the distance b, we can expand Eq. 3 to account for the individual absorption components for sand and fiber particles as:

$$A = \phi_s \alpha_s b + \phi_f \alpha_f b \tag{5}$$

where all variables were previously defined; the absorbance coefficient for the fibers was defined as $\alpha_f = \frac{4C_{\text{ext}f}}{\pi l d^2}$; and the subscripts s and f denote the sand and fiber, respectively. For the sand-fiber settling experiments, we assumed the extinction coefficient of fibers to be equal to the extinction efficiency of sand $Q_{\text{ext}_s} \approx Q_{\text{ext}_f}$, a valid assumption given the dimensions of the particles and fibers are much larger than the wavelength of the light-source (Bohren and Huffman, 2008). The extinction efficiency relates to the extinction cross-section by $Q_{\text{ext}} = \frac{C_{ext}}{A_{proj}}$, where A_{proj} is the projected area of the particle (i.e., sand grain or fiber). We further assumed that, due to the fiber orientation, the projected area of the fibers was that of a rectangle of dimensions ($l \times d$). Therefore, the fiber absorption coefficient can be estimated by

$$\alpha_f = \frac{4Q_{\text{ext}}}{\pi d} \tag{6}$$

We cannot estimate the local fiber concentration using our current experimental system. A zeroth-order approximation for the fiber concentration is to set the fiber concentration everywhere within the fracture equal to the overall fiber concentration of the suspension ($\phi_f = 0.0038$). This approximation underestimated fiber concentration within the sand-fiber pillars and overestimated fiber concentration in the solids-free regions. Therefore, we decided to use a first-order approximation of the fiber concentration by calculating the total area covered by solids and normalizing the bulk fiber concentration by this area. Such normalization was only applied in the regions identified as having solids: in solids-free regions $\phi_f = 0$ and in regions where solids were found, we set $\phi_f^* = \frac{\phi_f}{A_{\text{solids}}}$, here A_{solids} is defined as the fraction of the total area identified as having solids. Using the above analysis and assumptions yields

$$\phi_s = \frac{A - \alpha_f \phi_f^* b}{\alpha_s b} \tag{7}$$

where α_s was estimated in the constant-aperture experiment, α_f was estimated using Eq. 6, A was measured using light transmission techniques, and b was calculated by incrementally adjusting the aperture field to reflect the displacements recorded by the LVDTs. This analysis yields a robust quantitative measure of the solid volume fraction and gives a measure of the evolution of ϕ_s throughout the duration of the experiment. Fig. 4 shows a snapshot (subset) of these ϕ_s-fields at different times throughout the experiments.

4. ANALYSIS OF RESULTS

The displacement data for all experiments is shown in Fig. 3. The initial aperture is at zero displacement, positive displacement indicates aperture reduction, and a negative displacement indicates aperture increase. Test A (Fig. 3a) shows that the fracture opened slightly as fluid was injected into the fracture; however, the fracture returned to its original state (± 3 μm) after flow ceased. From test A and previously conducted experiments, we observed the formation of sand-fiber islands at early times, possibly formed during suspension injection or mixing. During the settling process, these sand-fiber islands eventually become immobilized. Over time, the sand-fiber islands on the upper regions may settle over islands located on the lower regions, which leads to the formation of larger islands with some particle-free regions trapped between them. The suspension is allowed to settle for approximately 140 minutes before injecting solids-free carrier fluid mimicking fluid flowback. We injected approximately 10 fracture volumes of carrier fluid into the fracture, which flushed the fiber-sand islands (along with much of the solids).

Tests B through D were initialized in the same manner as test A, however, after allowing the suspension to settle for 25 minutes, we applied a normal stress of σ_n =1.8 psi (12.4 kPa). The normal stress was then increased in regular intervals of $\Delta\sigma_n$ =1.8 psi approximately every 50 minutes to a maximum normal stress of σ_n =12.8 psi (88.3 kPa). Recorded LVDT displacements for the σ_n experiments show that the fracture opens during the injection process (see insert in Figs. 3b, 3c, and 3d) and slowly returns to its initial state after flow ceased. Recorded LVDT displacements show that during the first applied stress (σ_n =1.8 psi) fracture aperture decreased by $\sim$ 100μm; however, after the normal stress was increased (σ_n >1.8 psi), the fracture aperture decreased significantly. For test B, when the normal stress was increased to σ_n =3.6 psi, the fracture aperture decreased significantly ($1-1.5$ mm). Displacement data show the upper fracture surface began to deform nonuniformly, i.e., aperture on the upper-region of the fracture (LVDT 3 and 4) decreased more than re-

gions near the bottom of the fracture (LVDT 1 and 2). This nonuniform displacement of the fracture surface is consistent with the settling patterns observed in Fig. 4, in that the solid content in the lower region of the fracture was substantially higher than solid content in the upper region. This same behavior was observed in both test C and D but at a higher normal stress (σ_n =5.5 psi). The recorded displacements from test B-D show that, at the maximum applied stress (σ_n =12.8 psi), the aperture can decrease by up to $\sim$ 85% in the upper region, due to the relative absence of solids. By contrast, in the lower region of the fracture, we observed an aperture reduction of $\sim$ 40% at the maximum applied stress.

Solids-free carrier fluid was injected at time T=430 min (test B), T=480 min (test C), and T=405 min (test D). The displacement data from test B and C show that there is only a minimal change after flowback. Initially, the fracture in test D only deformed slightly during flowback; however, the outlet tubes were inadvertently closed/blocked-off which caused a temporary pressure increase inside the fracture. This pressure increase caused the fracture aperture to increase reaching values close to the original aperture; consequently, most of the solids were flushed out of the fracture.

Fig. 4 shows a snapshot of the ϕ_s-field for test A, B, and D, as the solids settled and as σ_n increased. For clarity and brevity, we omitted images for test C which showed results that were qualitatively similar to those of test B and D. The first row of Fig. 4 shows the ϕ_s-field shortly after suspension injection stopped. The second row shows the ϕ_s distribution 25 minutes into the settling process, i.e., just before applying a normal stress to the fracture on test B and D. The results for test A show that the sand-fiber islands were formed during the early-stage of the experiment, as previously mentioned. Subsequent frames (T = 25-140 min) show that the sand-fiber pillars settle in place early-on and experience only minimal changes throughout time. These pillars have an approximate solid volume fraction of $\sim 0.2 - 0.35$; the top regions of these pillars have a slightly higher concentration, ~ 0.4, due to suspended sand particles settling in those regions. After the injection of solids-free carrier fluid, most of the solids are flushed out of the fracture (last frame of test A).

The first and second frames of both test B and D show the ϕ_s-field inside the fracture and demonstrate, at least qualitatively, the reproducibility of our experimental procedure. As the normal stress increased, fracture aperture decreased. It was then observed that the fiber-sand islands that formed at early times compressed, forming sand-fiber pillars that prevented fracture closure. The aperture reduction forced sand-particles to rearrange, which displaced

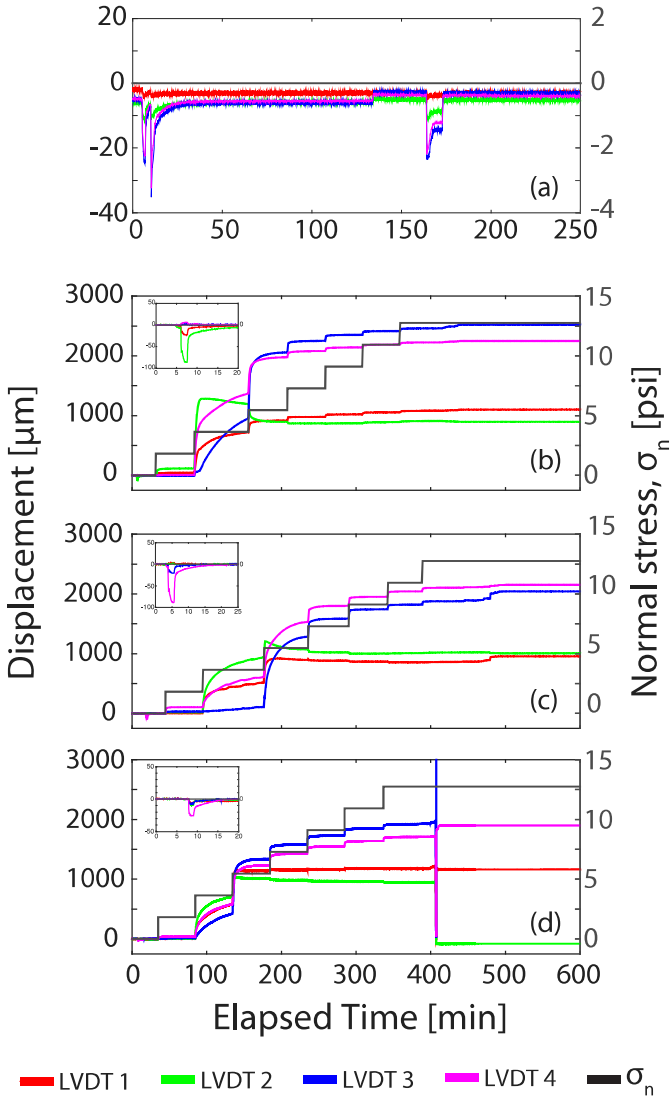

Fig. 3: Displacement data for all experiments; a positive displacement indicates fracture closure. (a) Test A: the suspension was injected around minute 5, which caused the fracture to temporarily open; after suspension injection was stopped, the fracture returns to its original position. Solids-free carrier fluid was injected after 140 minutes. (b-d) Displacement data for tests B-D, respectively. The black line shows the applied normal stress, and the colored lines correspond to the LVDT locations as indicated in Fig. 2.

fluid between sand grains and increased ϕ_s at the local scale (within the pillars). Fig. 4 shows that the solid concentration of the pillars increased after σ_n was increased with most regions reaching a solid volume fraction of $\phi_s \sim 0.6 - 0.75$, which is within the range of expected values for the random close packing limit $\phi_{\text{rcp}} \approx 0.65$ and close packing limit $\phi_{\text{cpl}} \approx 0.75$ (Santiso and Müller, 2002; Shapiro and Probstein, 1992). Pillars located in the top regions of the fracture (in test B and D) have slightly higher solid concentration $\phi_s \sim 0.8 - 0.85$, reaching the maximum packing limit $\phi_{\text{max}} \approx 0.84$ for nonuniform (bidisperse) solid distributions (Santiso and Müller, 2002).

Higher ϕ_s in these regions suggests that the fiber volume fraction might be higher than the estimated ϕ_f^*.

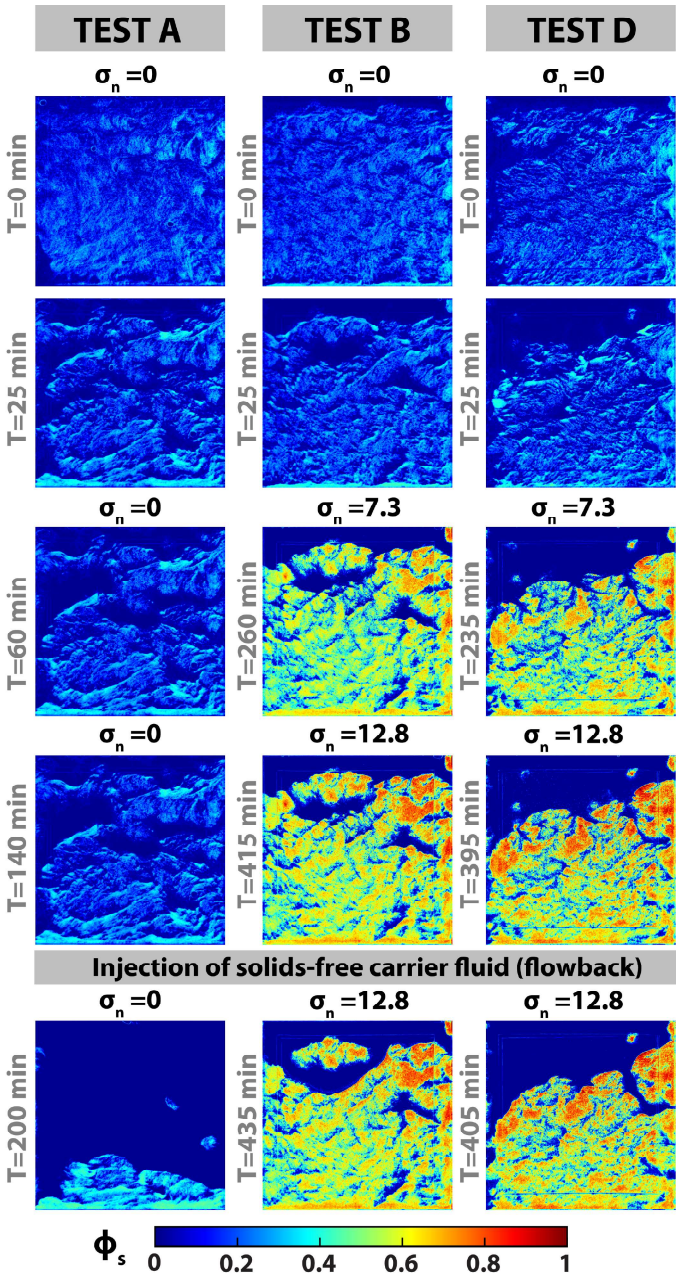

Fig. 4: Solid volume fraction (ϕ_s) distribution for test A (left column), test B (middle column), and test D (right column). The suspension in test A was allowed to settle without an applied normal stress, for approximately 2.5 hours before the flowback experiment was conducted. Tests B and D were allowed to settle for ~25 minutes before the normal stress was applied; after that, we increased the applied normal stress in regular increments of 1.8 psi up to a maximum normal stress of 12.8 psi every ~50 minutes.

5. DISCUSSION

A suspension of fibers and rod-like particles has been shown to reduce the settling velocity of a single particle falling through such suspension, both experimentally (Elgaddafi et al., 2012) and numerically (Harlen et al., 1999). There is evidence suggesting that such velocity reduction is due to the viscosity increase attributed to the addition of fibers (Guo et al., 2015; Milliken et al., 1989). Additionally, numerical simulations by Harlen et al. (1999) suggested that even at low fiber concentrations, the fiber-fiber contacts have an effect on the settling particle of the same order of magnitude as hydrodynamic interactions. The effect of such fiber-fiber contacts is predicted to increase in the presence of fiber-fiber networks with the polymer-chains as described in Section 1. When the smallest length-scale in the geometry is of the same order of magnitude as the fiber length, the fiber-fiber contacts become more significant. These fiber contacts are therefore an important aspect in the formation of the sand-fiber pillars. Previous preliminary experiments, conducted inside a constant-aperture fracture with small aperture to fiber-length ratio $b/l_f \sim 1/3 - 1/2$, demonstrated that the contacts between fiber-fiber, fiber-sand, and solid-walls dominated the settling process and completely hindered particle settling, i.e., sand particles settled in small regions (islands) surrounded by particle-free regions.

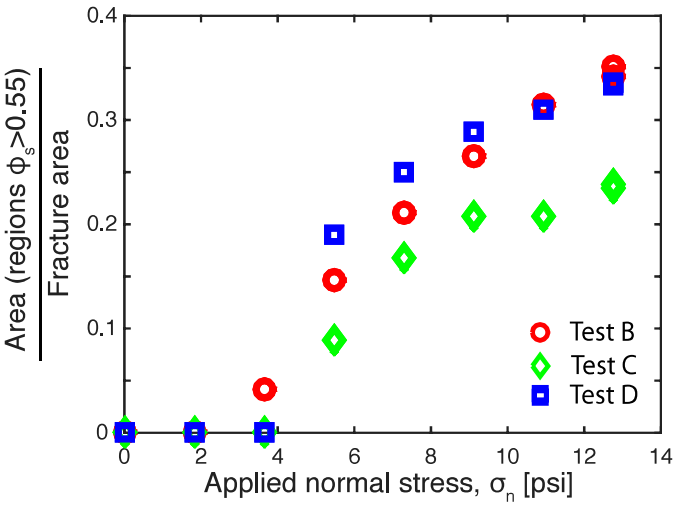

Fig. 5: Relative area for all regions with $\phi > 0.55$ plotted versus applied normal stress. As the applied normal stress increased, the area of regions with $\phi_s > 0.55$ increased, which was attributed to the sand grains compacting, caused by the aperture decrease.

The formation of the previously mentioned sand-fiber pillars suggests that the fracture permeability can increase by adding fibers to the suspension. However, the permeability enhancement is dependent on two factors: (1) the interconnectivity of the particle-free regions and (2) the ability of the sand-fiber pillars to support an applied normal stress ($\geq$ to the least principal normal stress), so as to prevent fracture closure. It was expected that as σ_n increased, the sand particles within the pillars would shift and rearrange into tighter packing. The formation

of tightly packed sand-fiber islands, coupled with the reduced fracture aperture, increased the contact points between particles and also increased the local solid volume fraction within the pillars ϕ_{pillars}. We took $\phi_{\text{rlp}} \approx 0.55$ (the random loose packing limit) as the minimum ϕ that can support an external load (Onoda and Liniger, 1990). Using the analysis described in Section 3 we were able to estimate the extent of the regions that were supporting the applied normal stress. Fig. 5 shows the evolution of the fraction of the total area covered by the regions with $\phi_s > 0.55$. As the normal stress increased the total area covered by these regions increased, reaching a maximum of ~ 0.35 for tests B and D, while the maximum area for test C was ~ 0.24. The increase in area suggests that solid particles within the sand-fiber pillars re-arrange causing the pillars to compact. Additionally, fluid between sand grains may be displaced due to the aperture reduction, and consequently particle compaction, which is manifested as an increase in area of the regions with $\phi_s > 0.55$.

Fig. 6 shows the normalized semi variograms for all frames shown in Fig. 4. The semi variogram, γ, provides a measure of the spatial correlation of the sand-fiber pillars. We normalized γ by the variance σ^2 of the ϕ_s-field to compare between experiments. For the experiment with zero normal stress, $\sigma_n = 0$, (test A), the solid distribution varied by a small amount over time (light gray to dark gray). After the solids were washed out of the fracture (flowback), there was a significant change in the spatial distribution of solids. Therefore, differences in spatial statistics for test B and test D can be directly related to the increased normal-stress applied to the system. Variograms for tests B and D show only minimal changes after flowback (black lines). All cases showed mild anisotropy which reflected the orientability of the fibers; the long axis of the fibers will tend to orient parallel to the direction of flow (x-direction in our experiments). As the applied stress increased, the correlation length increased and was related to the size of the sand-fiber pillars.

6. CONCLUSIONS

We have developed a new experimental system that allowed for the qualitative and quantitative analysis of a semi-dilute sand-fiber suspension settling inside a variable aperture fracture. The applied-normal-stress fracture system we developed yields reproducible initial conditions with solids distributed throughout the fracture area. We have demonstrated that an applied-normal-stress (σ_n) caused the sand particles to rearrange and form tightly packed pillars; additionally, as σ_n increased, the total area of regions with $\phi_s > 0.55$ increased. Using light transmission techniques gave a measure of the solid volume fraction of the pillars, and we found that these sand-fiber pillars have a solid volume fraction, ϕ_s, significantly higher than the solid content of the original mixture ($\phi_{\text{pillars}} > \phi_{\text{total}}$). After injecting solids-free carrier fluid we observed that some solids were washed away; however, the sand-fiber pillars remained largely unchanged. This created some large interconnected pathways, which suggest that the fracture permeability may, in fact, increase, aided by the formation of these sand-fiber pillars. We have demonstrated that the addition of fibers, even at low concentrations, has the potential to significantly increase fracture permeability.

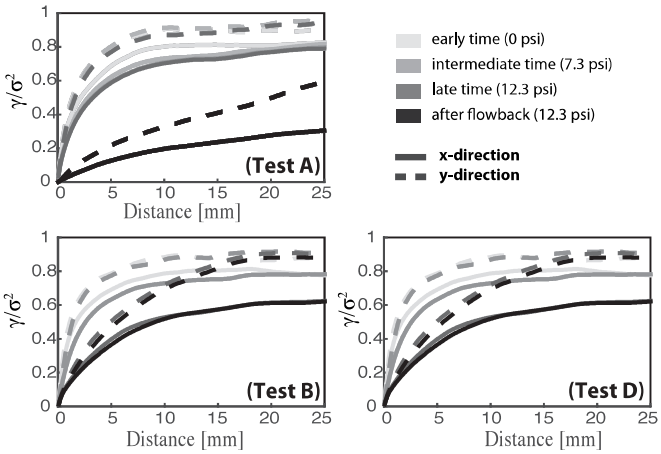

Fig. 6: Variograms of the ϕ_s-fields shown in Fig. 4. The variogram γ was normalized by the variance,σ^2, of the $\phi-$field.

REFERENCES

[1] T. Baldock, M. Tomkins, P. Nielsen, and M. Hughes. Settling velocity of sediments at high concentrations. *Coastal Engineering*, 51, no. 1 (2004), 91 –100.

[2] C. F. Bohren and D. R. Huffman. Absorption and scattering of light by small particles. John Wiley & Sons, 2008.

[3] R. Chhabra and S. Peri. Simple method for the estimation of free-fall velocity of spherical particles in power law liquids. *Powder Technology*, 67, no. 3 (1991), 287 –290.

[4] R. L. Detwiler, S. E. Pringle, and R. J. Glass. Measurement of fracture aperture fields using transmitted light: An evaluation of measurement errors and their influence on simulations of flow and transport through a single fracture. *Water Resources Research*, 35, no. 9 (1999), 2605–2617.

[5] R. Elgaddafi, R. Ahmed, M. George, and F. Growcock. Settling behavior of spherical particles in fiber-containing drilling fluids. *Journal of Petroleum Science and Engineering*, 84-85 (2012), 20–28.

[6] M. George, R. Ahmed, and F. Growcock. Rheological Properties of Fiber-Containing Drilling Sweeps at Ambient and Elevated Temperatures. *Proceedings of the 2011 National Technical Conference and Exhibition - American Association of Drilling Engineers*. 2011.

[7] M. George, R. Ahmed, and F. Growcock. "Stability and Flow Behavior of Fiber-Containing Drilling Sweeps". *Rheology*. Ed. by J. De Vicente. INTECH Open Access Publisher, 2012. Chap. 9.

[8] É. Guazzelli and J. Hinch. Fluctuations and Instability in Sedimentation. *Annual Review of Fluid Mechanics*, 43, no. 1 (2011), 97–116.

[9] J. Guo, J. Ma, Z. Zhao, and Y. Gao. Effect of fiber on the rheological property of fracturing fluid. *Journal of Natural Gas Science and Engineering*, 23, no. 0 (2015), 356 –362.

[10] R. Guo, J. Azaiez, and C. Bellehumeur. Rheology of fiber filled polymer melts: Role of fiber-fiber interactions and polymer-fiber coupling. *Polymer Engineering & Science*, 45, no. 3 (2005), 385–399.

[11] J. Happel and E. Bart. The settling of a sphere along the axis of a long square duct at low Reynolds' number. English. *Applied Scientific Research*, 29, no. 1 (1974), 241–258.

[12] O. G. Harlen, R. R. Sundararajakumar, and D. L. Koch. Numerical simulations of a sphere settling through a suspension of neutrally buoyant fibres. *Journal of Fluid Mechanics*, 388 (1999), 355–388.

[13] B. Herzhaft and É. Guazzelli. Experimental study of the sedimentation of dilute and semi-dilute suspensions of fibres. *Journal of Fluid Mechanics*, 384 (1999), 133–158.

[14] B. Herzhaft, E. Guazzelli, M. B. Mackaplow, and E. S. G. Shaqfeh. Experimental Investigation of the Sedimentation of a Dilute Fiber Suspension. *Phys. Rev. Lett.*, 77 (2 1996), 290–293.

[15] B. Lecampion and D. I. Garagash. Confined flow of suspensions modelled by a frictional rheology. *Journal of Fluid Mechanics*, 759 (2014), 197–235.

[16] R. Medina, J. E. Elkhoury, J. P. Morris, R. Prioul, J. Desroches, and R. L. Detwiler. Flow of concentrated suspensions through fractures: small variations in solid concentration cause significant in-plane velocity variations. *Geofluids*, 15, no. 1-2 (2015), 24–36.

[17] W. J. Milliken, M. Gottlieb, A. L. Graham, L. A. Mondy, and R. L. Powell. The viscosity-volume fraction relation for suspensions of rod-like particles by falling-ball rheometry. *Journal of Fluid Mechanics*, 202 (1989), 217–232.

[18] G. Y. Onoda and E. G. Liniger. Random loose packings of uniform spheres and the dilatancy onset. *Phys. Rev. Lett.*, 64 (22 1990), 2727–2730.

[19] M. Rajabian, C. Dubois, M. Grmela, and P. Carreau. Effects of polymer–fiber interactions on rheology and flow behavior of suspensions of semi-flexible fibers in polymeric liquids. *Rheologica Acta*, 47, no. 7 (2008), 701–717.

[20] E. Santiso and E. A. Müller. Dense packing of binary and polydisperse hard spheres. *Molecular Physics*, 100, no. 15 (2002), 2461–2469.

[21] A. P. Shapiro and R. F. Probstein. Random packings of spheres and fluidity limits of monodisperse and bidisperse suspensions. *Phys. Rev. Lett.*, 68 (9 1992), 1422–1425.